Electrochimica Acta 179 (2015) 146–153

Contents lists available at ScienceDirect

Electrochimica Acta

journal homepage: www.elsevier.com/locate/electacta

Tantalum oxide-based electrocatalysts made from oxy-tantalum phthalocyanines as non-platinum cathodes for polymer electrolyte fuel cells

N. Uehara [a], A. Ishihara [b,*], M. Matsumoto [c], H. Imai [c], Y. Kohno [a], K. Matsuzawa [a], S. Mitsushima [a,b], K. Ota [a]

[a] Green Hydrogen Research Center, Yokohama National University 79-5, Tokiwadai, Hodogaya-ku, Yokohama 240-8501, JAPAN
[b] Institute of Advanced Sciences, Yokohama National University 79-5, Tokiwadai, Hodogaya-ku, Yokohama 240-8501, JAPAN
[c] NISSAN ARC Ltd. 1 Natsushima-cho, Yokosuka 237-0061, JAPAN

ARTICLE INFO

Article history:
Received 24 December 2014
Received in revised form 13 March 2015
Accepted 17 March 2015
Available online 19 March 2015

Keywords:
polymer electrolyte fuel cell
non-platinum cathode
oxygen reduction reaction
tantalum oxide
oxygen vacancy

ABSTRACT

The development of non-platinum-based cathodes is required in order to commercialize polymer electrolyte fuel cells. We have previously investigated group 4 and 5 transition metal oxides because they exhibit high chemical stability under cathode conditions and are less costly than platinum. In this paper, tantalum oxide-based cathodes were prepared from oxy-tantalum phthalocyanines by heat treatment under low oxygen partial pressures. We successfully obtained nano-sized tantalum oxide-based particles dispersed on multi-walled carbon nanotubes to increase the oxygen reduction reaction (ORR) current density. We investigated the factors which influence ORR activity in terms of the onset potential and ORR current density. The onset potential increased with increasing crystalline distortion of orthorhombic Ta_2O_5, which was experimentally observed as changes in the position and full width at half maximum of the Ta_2O_5 (0 0 1) peak in the X-ray diffraction patterns. In addition, the amount of the deposited carbon strongly influenced the ORR current density because it affected the surface area of the oxides and the formation of local electron conduction paths.

1. Introduction

Polymer electrolyte fuel cells (PEFCs) offer many advantages including high power densities, high energy conversion efficiencies, and lower operating temperatures. They are therefore suitable as power sources for vehicles and residential cogeneration power systems. However, the use of Pt as a cathode electrocatalyst for PEFCs is a problem because of its high cost, limited availability, and insufficient stability. To successfully commercialize PEFCs, low-cost non-platinum cathode catalysts with high stability must be developed. Iron- and/or cobalt-complex-based catalysts such as Fe–N–C [1], carbon-based catalysts [2], and chalcogenides [3] have been investigated as non-platinum cathode catalysts under cathode conditions for PEFCs. Recently, Cheon et al. reported that the oxygen reduction reaction (ORR) activities of Fe- and Co-doped ordered mesoporous porphyrinic carbons were greater than that of platinum [4]. However, these catalysts were unstable under cathode conditions, which include a severely corrosive (e.g. acidic) environment and oxidative atmosphere.

We have focused on Group 4 and 5 transition metal oxide-based compounds because of their high chemical stabilities under cathode conditions. We have previously described the acid stability and catalytic ORR activity for a number of materials, including tantalum-doped tungsten carbide [5], tantalum oxynitride [6–8], zirconium oxide [9–11], titanium oxide [12], zirconium oxynitride [13,14], tantalum carbonitride [15], and tantalum-oxide- or zirconium-oxide-based catalysts [16–18]. In addition, we revealed that the tantalum oxide-based catalysts prepared from tantalum carbonitride by heat treatment under low oxygen partial pressure showed definite ORR activity, and identified the active sites as oxygen vacancies on the oxide [19].

Unfortunately, the tantalum carbonitride precursors in the aforementioned work had small surface areas because they were prepared via heat treatment at high temperature (around 2000 K). Therefore, the surface areas of the oxide-based catalysts prepared by heat treatment under low oxygen partial pressures remained as low as several $m^2 g^{-1}$ [16]. However, the carbon and nitrogen components of the carbonitride precursors are considered to be

* Corresponding author.

http://dx.doi.org/10.1016/j.electacta.2015.03.125
0013-4686/

effective for creating the oxygen-vacancy active sites [19]. Thus, an investigation of new methods for the synthesis of the oxide-based catalysts, which would increase the ORR current by increasing the surface areas of the catalysts, is warranted.

In this study, we prepared tantalum oxide nanoparticles using the organometallic complex oxy-tantalum phthalocyanine (TaOPc) as a precursor. We used multiwalled carbon nanotubes (MWCNTs) as both the support and electrical conductive material to form macro electron conduction paths in the catalyst powders. In addition, we investigated the relationship between the physico-chemical properties and ORR activity (such as onset potential and ORR current density) to clarify the factors which influence the ORR activity.

2. Experimental

2.1. Catalyst preparation

Oxy-tantalum phthalocyanine (TaOPc [$TaOC_{32}H_{16}N_8$], Dainichi-seika Color & Chemicals Mfg. Co., Ltd) was used as the starting material. The TaOPc (0.6 g) and MWCNTs (0.256 g, diameter = 10–15 nm, length = 3 μm) as a conductive material were dry ball milled with 180 chrome steel balls (5 mm in diameter) for 3 h at 400 rpm. The powders and balls were separated by sieving and the powders were ground in a mortar to obtain the catalyst precursor (TaOPc/MWCNT). The catalyst precursor was placed in a quartz tube and heated from room temperature to 900 °C at 20 °C/min under inert N_2 atmosphere. When the temperature reached 900 °C, a reactive gas mixture consisting of 2% H_2 with either 0.5 or 0.05% O_2 was introduced and continuously supplied at 1.7×10^{-6} $m^3 \cdot s^{-1}$ for 0.5 – 15 h. During this heat treatment, the precursor was oxidized gradually to form tantalum oxide. This oxidation process under low oxygen partial pressure is denoted as LO, and the heat treatment time is termed the oxidation time. The obtained catalysts are designated in the form "$TaC_xN_yO_z$/MWCNT_oxygen partial pressure-oxidation time", as for example, $TaC_xN_yO_z$/MWCNT_0.05%O_2–10 h. $TaC_xN_yO_z$ indicates that the compound has tantalum oxide structures and contains both C and N. X-ray diffraction spectroscopy (XRD; Rigaku Ultima IV, X-ray source: CuKα) was performed to reveal the crystalline structure, peak position, and full width at half maximum (FWHM) of the catalysts. X-ray photoelectron spectroscopy (XPS; PHI Quantum-2000, X-ray source: monochromated AlKα radiation) was used to reveal the valence of the tantalum at the surface of the tantalum oxide. Transmission electron microscopy (TEM; JEOL LEM-2100F) and scanning electron microscopy (SEM; JEOL JSM-7100F) were used to observe the morphology of the catalysts.

2.2. Electrode preparation

2.2.1. Stationary electrode

We used a stationary electrode system to accurately evaluate the onset potential instead of a rotating ring-disk electrode (RRDE), because the noise produced by the latter interfered with the accurate determination of the onset potential.

Catalyst powder (3 mg) was mixed in a 1:1 (mass ratio) solution of 1-propanol and distilled water (0.15 dm^3) with 0.5 wt% Nafion® solution (5 mm^3) to prepare a catalyst ink. The catalyst ink was repeatedly dropped on a polished glassy carbon rod (GC; φ = 5.2 mm) and dried at 60 °C until the oxides in the powder catalyst were supported at a loading of ca. 0.37 – 0.51 $mg \cdot cm^2$ on top of the GC.

2.2.2. Rotating ring-disk electrode (RRDE)

The RRDE consisted of a glassy carbon disk (6.0 mm in diameter) surrounded by a platinum ring with an internal diameter of 7.0 mm and an external diameter of 9.0 mm. Catalyst powder (2.45 mg) was mixed into a solution of 1-hexanol (0.10 dm^3) and 5 wt% Nafion® solution (4 mm^3) to prepare a catalyst ink. The catalyst ink (15 mm^3) was dropped on the polished disk of the RRDE and dried at 50 °C. The loading of the oxides in the powder catalyst on the RRDE was ca. 0.51–0.57 $mg \cdot cm^2$.

2.3. Electrochemical measurements

The stationary electrode measurements were performed with a 3-electrode cell and the RRDE measurements were performed with a RRDE cell. Both cells contained 0.1 mol dm^3 H_2SO_4 at 30 °C. A reversible hydrogen electrode (RHE) and a glassy carbon plate were used as the reference and counter electrodes, respectively. Slow scan voltammetry (SSV) was performed at a scan rate of 5 $mV \cdot s^{-1}$ from 0.2 to 1.2 V under O_2 and N_2 atmospheres. In the case of the RRDE measurements, the electrode rotation was set at 1600 rpm and the ring electrode was set at 1.2 V during SSV. The current density of oxygen reduction, j_{ORR}, was obtained by taking the difference between the third cycle SSV measurements in N_2 and O_2. The current density was based on the weight of the oxides: $mA \cdot g^{-1}$. For the evaluation of catalyst activity, we used the j_{ORR} at 0.8 V vs. RHE ($|j_{ORR}$@0.8 V|) and the potential at 5 $mA \cdot g^{-1}$ (E_{ORR}@5 $mA \cdot g^{-1}$) as the onset potential.

3. Results and discussion

During the preparation of the catalyst, we used chrome steel balls in the ball-milling step. However, there appeared to be no effect of Fe on the ORR activity because the j_{ORR} values for $TaC_xN_yO_z$/MWCNT_0.5%O_2-1 h samples prepared with either chrome steel or zirconia balls were nearly the same, as shown in Fig. S1 (Supplementary Information). Fig. 1 shows the j_{ORR} (normalized to oxide mass) versus E curves for $TaC_xN_yO_z$ (CN) made from tantalum carbonitride [19], $TaC_xN_yO_z$/MWCNT_0.5%O_2-1 h, and 0.05%O_2-10 h (We must express exactly as $TaC_xN_yO_z$/MWCNT_0.05%O_2-10 h, however, omit it 0.05%O_2-10 h when it is clear) as stationary electrodes. The total amount of supplied oxygen in the case of $TaC_xN_yO_z$/MWCNT_0.5%O_2-1 h was same as that of 0.05%O_2-10 h. The ORR currents of the $TaC_xN_yO_z$/MWCNT_0.5%O_2-1 h and 0.05%O_2-10 h started to flow at around 0.9 V. The E_{ORR}@5 $mA \cdot g^{-1}$ values of the $TaC_xN_yO_z$/MWCNT_0.5%O_2-1 h and 0.05%O_2-10 h materials were 0.894 and 0.875 V vs. RHE, and the $|j_{ORR}$@0.8 V| values were ca. 463 and 310 $mA \cdot g^{-1}$, respectively. The $TaC_xN_yO_z$/MWCNT(CN) exhibited ca. 9 $mA \cdot g^{-1}$ at 0.8 V as a maximum value. Thus, the $|j_{ORR}$@0.8 V| values for the

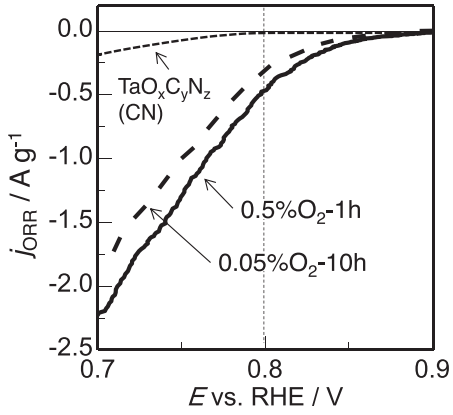

Fig. 1. j_{ORR} (normalized to oxide mass) – E curves for the $TaC_xN_yO_z$(CN) samples made from tantalum carbonitride, $TaC_xN_yO_z$/MWCNT_0.5%O_2-1 h, and $TaC_xN_yO_z$/MWCNT_0.05%O_2-10 h as stationary electrodes.

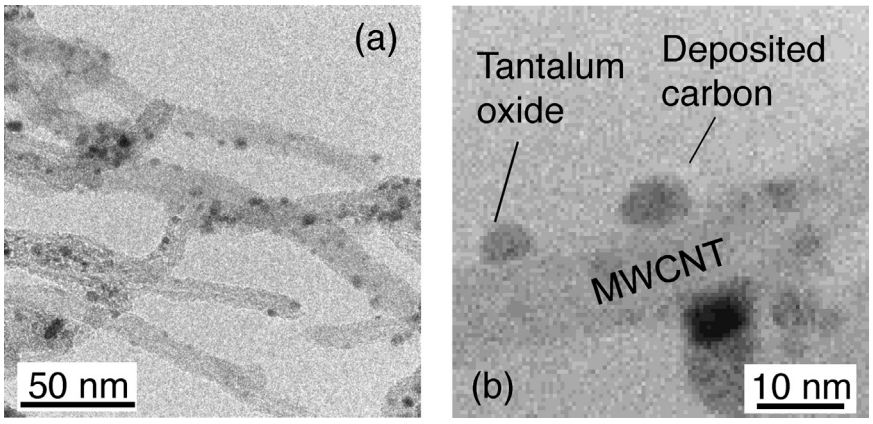

Fig. 2. TEM images of $TaC_xN_yO_z$/MWCNT_0.5%O_2-1 h at (a) low and (b) high magnification.

$TaC_xN_yO_z$/MWCNTs made from TaOPc were about 50 times higher. As described previously, hydrogen reacts with oxygen to produce water to maintain the low oxygen partial pressure [19]. Indeed, the catalyst made by heat treatment without hydrogen was white, indicating that the tantalum oxide was relatively oxidized (Fig. S2). The equilibrium partial pressures of oxygen in the 2% H_2 mixtures with 0.5% and 0.05% O_2 were calculated to be 4.4×10^{-12} and 1.3×10^{-14} Pa, respectively. Despite the very low partial oxygen pressure, tantalum compounds such as the nitrides and carbides are thermochemically oxidized to Ta_2O_5. The decomposition of TaOPc occurs during the temperature increase to 900 °C, and the oxidation of the decomposed TaOPc gradually proceeds during the continued heat treatment at 900 °C under 2% H_2 + 0.5 or 0.05% O_2 atmosphere. As shown in Fig. 1, in spite of the same amount of supplied oxygen during LO, the $TaC_xN_yO_z$/MWCNT_0.5%O_2-1 h had higher ORR activity than the 0.05%O_2-10 h, indicating that the oxidation time, oxygen partial pressure, or both during LO influences the ORR activity of the $TaC_xN_yO_z$/MWCNTs.

Fig. 2(a) and (b) show TEM images of $TaC_xN_yO_z$/MWCNT_0.5% O_2-1 h. As shown in Fig. 2(a), the gray tubules are the MWCNT support and the black spots are tantalum oxide-based particles. The size of most of the tantalum oxide-based particles was well-controlled at nanometer scale, from 5 to 10 nm. In addition, the tantalum oxide-based nanoparticles were highly dispersed on the MWCNTs.

As shown in Fig. 2(b), the tantalum oxide-based particles were supported on the MWCNTs. In addition, the surface of the oxide-based particles was partially covered with a light-gray amorphous material, which was identified as the deposited amorphous carbon derived from the phthalocyanine structures. The deposited carbon seems to restrict the increase in the size of the oxide-based particles. In addition, the deposited carbon seems to form local electron conduction paths near the active sites. However, an excess of the deposited carbon would entirely cover the surface of the oxides and hinder the ORR. Therefore, to obtain a large ORR current, carbon deposition must be controlled to optimize the balance between the exposure of the oxide surface and the local electron conduction paths. Because we successfully prepared nano-sized tantalum oxide-based catalysts using TaOPc as the precursor, the ORR current was dramatically increased compared to that of $TaC_xN_yO_z$(CN) made from the carbonitride.

Fig. 3(a) and (b) show the dependence on the amount of the supplied oxygen during LO of the $|j_{ORR}$@0.8 V| and E_{ORR}@5 mA·g^{-1} values, respectively. In both measurements, $TaC_xN_yO_z$/MWCNT_0.5%O_2 showed higher catalytic activity than 0.05%O_2, suggesting that active sites with different properties were formed under the different partial pressures of oxygen.

As shown in Fig. 3(a), under both oxygen partial pressures, there was an optimum value (7 mmol g^{-1}, where the mass in the unit corresponds to the precursor, TaOPc/MWCNT) for the amount of supplied oxygen needed to obtain a high current density. In contrast, the E_{ORR}@5 mA·g^{-1} values of both $TaC_xN_yO_z$/MWCNTs became higher with decreasing amounts of supplied oxygen, as shown in Fig. 3(b). This tendency, which was apparently different from that of the $|j_{ORR}$@0.8 V|, suggested that the $|j_{ORR}$@0.8 V| and E_{ORR}@5 mA·g^{-1} values mainly reflect different properties of the active sites, that is, their quantity and quality, respectively. In general, since the $|j_{ORR}$@0.8 V| reflects the quantity of active sites, the surface area of the oxide-based particles was first considered as an influence on this parameter. However, the size of the

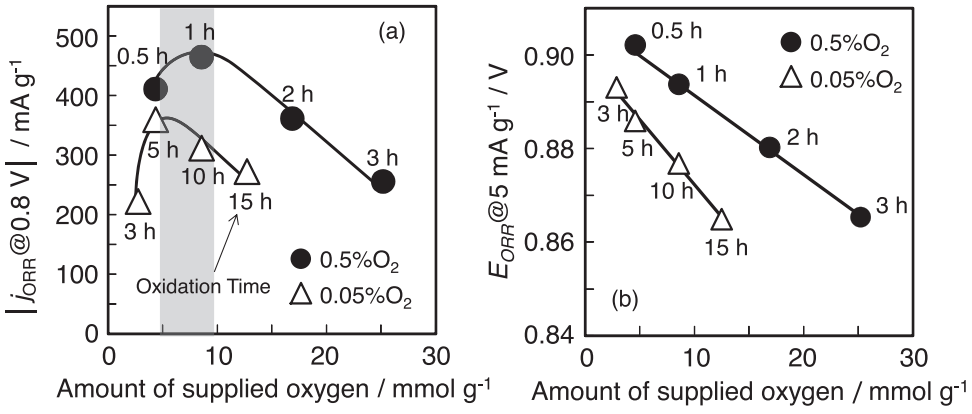

Fig. 3. Dependence of (a) $|j_{ORR}$@0.8 V| and (b) E_{ORR}@5 mA·g^{-1} values on the amount of supplied oxygen during LO.

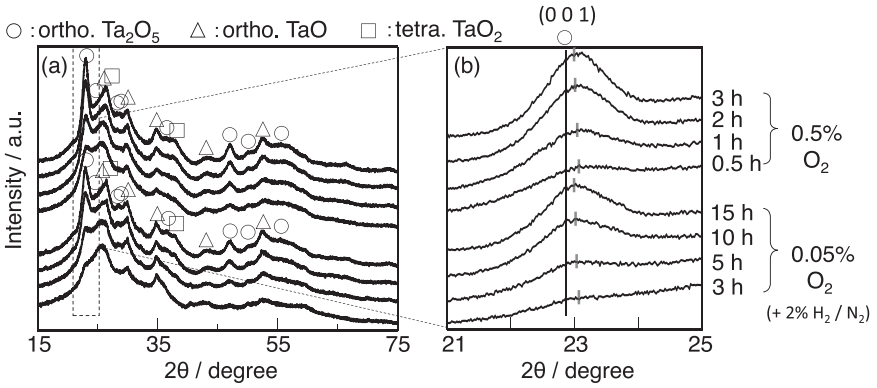

Fig. 4. XRD patterns of $TaC_xN_yO_z$/MWCNT_0.5%O_2 and $TaC_xN_yO_z$/MWCNT_0.05%O_2 over (a) a wide range (15–75°) and (b) a small range (21–25°).

oxide-based particles did not appear to change with oxidation time because the deposited carbon covered the particles and restricted their growth (Fig. S3). The tantalum oxide particle size distribution was determined with respect to time (Fig. S4). The average particle sizes of $TaC_xN_yO_z$/MWCNT_0.5%O_2-0.5 h, 1 h, and 3 h were 9.53, 9.64, and 9.99 nm, respectively. The sizes were nearly unchanged with increasing oxidation time. Hence, the $|j_{ORR}@0.8\,V|$ was affected by the deposited carbon which was gradually oxidized to CO and/or CO_2 during LO rather than the physicochemical properties of the oxides. In contrast, the $E_{ORR}@5\,mA{\cdot}g^{-1}$ was affected by the quality of the active sites, because it was defined with small ORR current density, that is, it was less affected by surface area of the oxides. Therefore, the $E_{ORR}@5\,mA{\cdot}g^{-1}$ values were mainly affected by the physicochemical properties of the oxides.

Fig. 4(a)shows the XRD patterns of $TaC_xN_yO_z$/MWCNT_0.5%O_2 and 0.05%O_2. The catalysts were composed of orthorhombic (ortho.) Ta_2O_5, ortho. TaO, and tetragonal TaO_2. No carbide, nitride, or carbonitride peaks appeared, revealing that all the $TaC_xN_yO_z$/MWCNTs were oxide-based compounds. The $TaC_xN_yO_z$/MWCNTs prepared with short oxidation times exhibited ortho. TaO and other broad peaks, indicating that low-valence tantalum oxides such as TaO with low crystallinity were formed by thermal decomposition of the TaOPc/MWCNTs. The ortho. TaO and tetra. TaO_2 were unstable and oxidized to Ta_2O_5 under the experimental conditions. In fact, the ortho. Ta_2O_5 peaks gradually grew as the oxidation time was extended. However, ortho. TaO peaks still remained even after the ortho. Ta_2O_5 peaks had considerably increased.

Fig. 5 shows the Ta 4*f* XPS spectra of the $TaC_xN_yO_z$/MWCNT_0.5%O_2-1 h and 0.05%O_2-10 h. The Ta 4*f* XPS spectra reveal that the surfaces of both materials consist mainly of ortho. Ta_2O_5, although the spectrum of the $TaC_xN_yO_z$/MWCNT_0.5%O_2-1 h sample is slightly shifted to lower binding energy. The XRD patterns revealed that the $TaC_xN_yO_z$/MWCNTs with longer oxidation times still contain ortho. TaO. The XRD and XPS results indicate that the oxygen in the reactive gas mixture might not have been able to reach ortho. TaO which was present in the MWCNT aggregates during LO. Since the ORR occurs on the surface, as detected by XPS, it is considered that the ORR active sites exist on the ortho. Ta_2O_5. Therefore, we focused on the main peak of ortho. Ta_2O_5 (Fig. 4(b)).

As shown in Fig. 4(b), it seems that the position of the ortho. Ta_2O_5 (0 0 1) peak shifts to higher angle when the oxidation time is shorter. In addition, the FWHM of the Ta_2O_5 (0 0 1) peak decreases with increasing oxidation time. This indicates that the crystallinity of the ortho. Ta_2O_5 increases with increasing oxidation time rather than the sizes of the oxides, which do not change over time. We then examined the peak separations in the XRD patterns (Fig. S5) to accurately evaluate the peak position and FWHM values of Ta_2O_5 (0 0 1) as a parameter for the crystallinity of Ta_2O_5.

We investigated the dependence of the position and FWHM of the Ta_2O_5 (0 0 1) peak on the amount of supplied oxygen in Figs. 6(a) and (b), respectively. We plotted the quantity of supplied oxygen along the *x*-axis instead of the oxidation time for both $TaC_xN_yO_z$/MWCNT_0.5%O_2 and 0.05%O_2. The oxidation times are specified in the figures. In Fig. 6(a), we could confirm that the peak position of Ta_2O_5 (0 0 1) shifted to higher angle with decreasing oxidation time. The peak at 22.9° corresponds to the peak position of commercial ortho. Ta_2O_5, so the large shift in the peak position away from 22.9° indicates that the crystalline distortion of ortho. Ta_2O_5 increases with decreasing oxidation time. Through the plots in Fig. 6(b), we confirmed that the FWHM of the Ta_2O_5 (0 0 1) peak widens with decreasing oxidation time. The FWHM of Ta_2O_5 (0 0 1) also reveals the degree of crystalline distortion in the ortho. Ta_2O_5. As a result, the crystalline distortion of ortho. Ta_2O_5 became larger with decreasing oxidation time in terms of both the peak shift and FWHM.

Next, we examined the relationship between the ORR activity and crystalline distortion of ortho. Ta_2O_5. The ORR activity was evaluated in terms of the $|j_{ORR}@0.8\,V|$ and $E_{ORR}@5\,mA{\cdot}g^{-1}$. The $|j_{ORR}@0.8\,V|$ is strongly dependent on the surface area of the oxides, which in turn is mainly affected by the deposited carbon covering the oxide surface as well as the particle size. The effect of the amount of the deposited carbon on the $|j_{ORR}@0.8\,V|$ will be discussed later. On the other hand, the $E_{ORR}@5\,mA{\cdot}g^{-1}$ is mainly reflected in the physicochemical properties of the oxides.

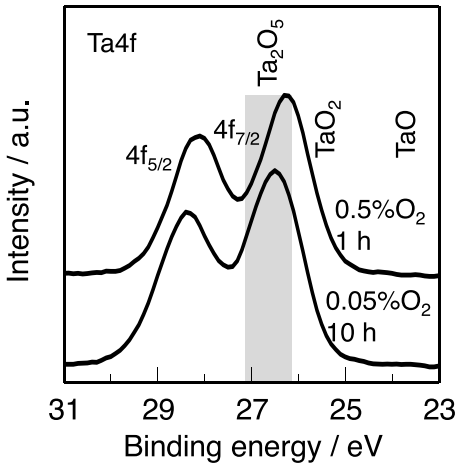

Fig. 5. Ta 4f XPS spectra of $TaC_xN_yO_z$/MWCNT_0.5%O_2-1 h and $TaC_xN_yO_z$/MWCNT_0.05%O_2-10 h.

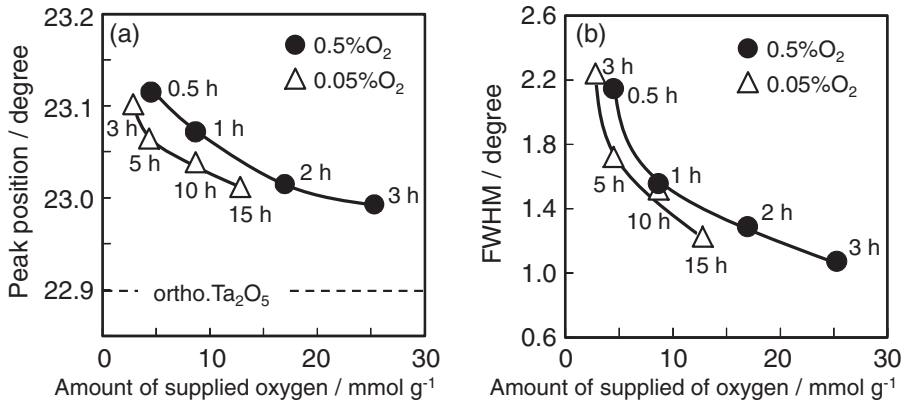

Fig. 6. Dependence of (a) peak position and (b) FWHM of ortho. Ta_2O_5 (0 0 1) on amount of supplied oxygen during LO.

Therefore, we investigated the relationship between E_{ORR}@5 mA·g^{-1} and the peak position and FWHM of Ta_2O_5 (0 0 1), as shown in Figs. 7(a) and (b). In both cases, the E_{ORR}@5 mA·g^{-1} increases with increases in the shift and FWHM of the Ta_2O_5 (0 0 1) peak, that is, concomitantly with the crystalline distortion of ortho. Ta_2O_5. A higher E_{ORR} means that the quality of the active sites improves. Hence, to understand the quality of the active sites, we carried out RRDE measurements.

Fig. 8(a) and (b) show the disk and ring current densities versus E curves for $TaC_xN_yO_z$/MWCNT_0.5%O_2 with different oxidation times at 0.2–1.2 V and a rotation rate of 1600 rpm. In Fig. 8(a), the ring current densities which are responsible for the production of hydrogen peroxide are observed near 0.8 V; these increase with extended oxidation times. In terms of ORR current densities (disk current densities, Fig. 8(b)), the $TaC_xN_yO_z$/MWCNT_0.5%O_2-1 h shows the highest value. We calculated the hydrogen peroxide formation rate, X_{H2O2}, from the disk and ring current densities in Fig. 8.

$$X_{H2O2} = (2j(\mathrm{geo})_{disk})/(Nj(\mathrm{geo})_{ring} + j(\mathrm{geo})_{disk}) \times 100 \quad (1)$$

where N is the collection efficiency of the RRDE measurement. The value of N was measured using an aqueous solution containing 1 mmol dm^{-3} $K_4[Fe(CN)_6]$ and 0.1 mol dm^{-3} K_2SO_4. The determined N was 0.337 when the rotation rate was 1600 rpm. Fig. 9 shows the X_{H2O2} – E curves of the $TaC_xN_yO_z$/MWCNTs for different oxidation times. The $TaC_xN_yO_z$/MWCNT_0.5%O_2-3 h catalyst affords the highest X_{H2O2}, while $TaC_xN_yO_z$/MWCNT_0.5%O_2-0.5 h results in the lowest value. The value of X_{H2O2} grows higher when the oxidation time is extended. This trend is similar to that of the E_{ORR}@5 mA·g^{-1}.

Next we examined the relationship between X_{H2O2}@0.6 V and E_{ORR}@5 mA·g^{-1}, as shown in Fig. 10; a linear relationship was observed between the two terms. This relationship was also observed at other potentials (e.g., 0.5, and 0.7 V) in terms of X_{H2O2}. The X_{H2O2} decreases as the E_{ORR}@5 mA·g^{-1} increases. A lower X_{H2O2} value means that the number of oxygen vacancies that can act as four-electron reduction sites is larger than those acting as two-electron reduction sites, i.e. the ratio four-electron reduction sites to two-electron reduction sites is large. Therefore, this result indicates that the preferential formation of ORR active sites where four-electron reduction occurs causes the E_{ORR}@5 mA·g^{-1} to rise. Considering that the E_{ORR}@5 mA·g^{-1} value increases with the increasing peak shift and FWHM values of Ta_2O_5 (0 0 1), that is, with the increase in the crystalline distortion of the ortho. Ta_2O_5, we can conclude that the increase in the crystalline distortion of ortho. Ta_2O_5 preferentially produces ORR active sites at which four-electron reduction occurs. In other words, the higher E_{ORR}@5 mA·g^{-1} is responsible for the improvement in the quality of the active sites. More extensive crystalline distortion is obtained at shorter oxidation times. The shorter oxidation times are

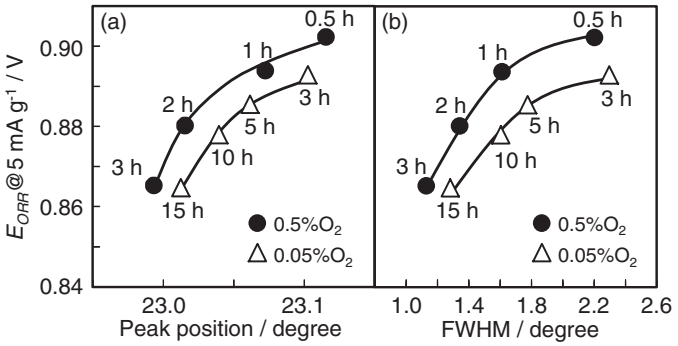

Fig. 7. Relationship between onset potential at 5 mA·g^{-1} and (a) peak position and (b) FWHM of ortho. Ta_2O_5 (0 0 1).

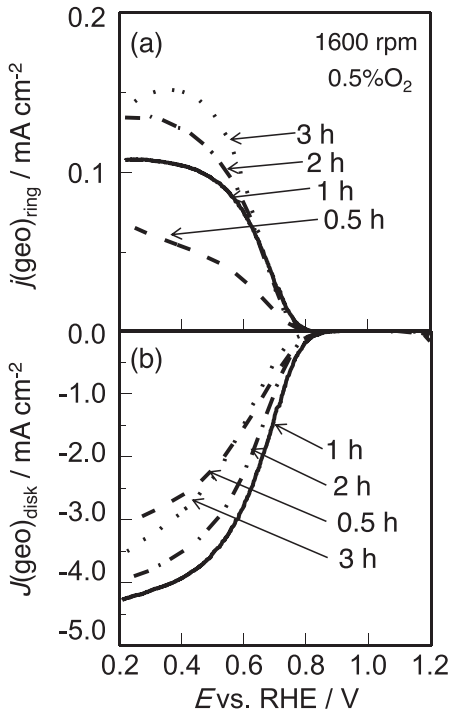

Fig. 8. (a) $j(\mathrm{geo})_{ring}$ – E and (b) $j(\mathrm{geo})_{disk}$ – E curves of $TaC_xN_yO_z$/MWCNT_0.5%O_2 for different oxidation times using RRDE electrodes. Rotation rate, 1600 rpm.

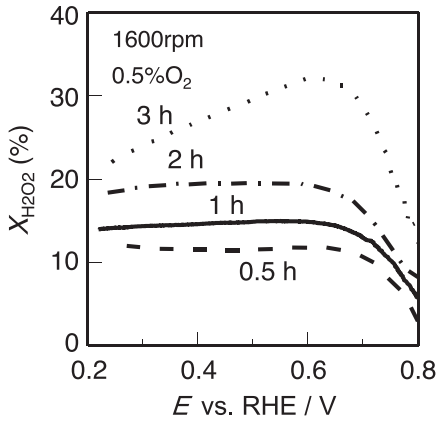

Fig. 9. X_{H2O2} – E curves of $TaC_xN_yO_z$/MWCNT_0.5%O_2 for different oxidation times using RRDE electrodes. Rotation rate, 1600 rpm.

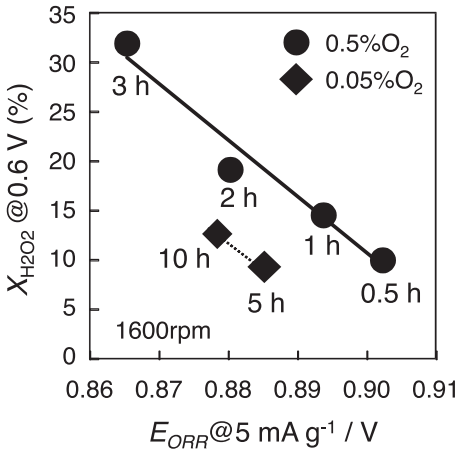

Fig. 10. Relationship between the onset potential at 5 mA·g^{-1} and X_{H2O2} at 0.6 V.

favourable for producing the oxygen vacancies because the amount of supplied oxygen is small and the heat treatment time is short.

On the other hand, differences in the results are observed depending on the partial pressure of the supplied oxygen. As shown in Fig. 3, both $|j_{ORR}$@0.8 V| and E_{ORR}@5 mA·g^{-1} are lower for the $TaC_xN_yO_z$/MWCNT_0.05%O_2 than those for 0.5%O_2. Furthermore, as shown in Figs. 7(a) and (b), although the positions and FWHM values of the ortho. Ta_2O_5 (0 0 1) peaks are the same, the E_{ORR}@5 mA·g^{-1} of $TaC_xN_yO_z$/MWCNT_0.5%O_2 is higher than that of 0.05%O_2. These results suggest that active sites with entirely different structures are probably formed during the oxidation at different oxygen partial pressures. The difference is apparent in the XPS spectra, as shown in Fig. 5. The Ta 4*f* spectra of $TaC_xN_yO_z$/MWCNT_0.5%O_2 slightly shifted lower binding energy than that of 0.05%O_2. However, this difference will be analysed in detail and discussed in a forthcoming paper. Here, we found that heat treatment of the decomposed TaOPc for a short time (ca. 0.5–1 h) under high oxygen partial pressure (0.5% O_2) is favourable for obtaining highly ORR-active tantalum oxide-based catalysts.

Next, we investigated the relationship between the ORR current density and the physicochemical properties of the catalysts. The ORR current density is strongly affected by the surface area of the oxides and the electron conduction paths, as well as the quality of the active sites. We examined the deposited carbon derived from phthalocyanine which forms the local electron conduction paths at the oxide surface. Fig. 11 shows the SEM images of $TaC_xN_yO_z$/MWCNT_0.5%O_2 and 0.05%O_2 after various oxidation times. When the oxidation time was short (Fig. 11(a) and (d)), the MWCNTs and tantalum oxides were almost covered with deposited carbon. As the oxidation time was prolonged (Fig. 11(a)→(b)→(c) and (d)→(e)→(f)), the MWCNTs and the tantalum oxide particles could be clearly observed because the deposited carbon was oxidized to form CO and/or CO_2 during LO. High magnification SEM images of the two materials after various oxidation times are shown in Fig. S3. These figures also show the removal of deposited carbon, allowing clear visualization of the oxide particles.

To quantitatively evaluate the amount of deposited carbon, we calculated the composition of the $TaC_xN_yO_z$/MWCNTs, which consist of the tantalum oxides, MWCNTs, and deposited carbon. The compositions of the catalysts were calculated as follows. First, the carbon in the $TaC_xN_yO_z$/MWCNT was completely burned by heating the catalyst at 800 °C in air. The residual weight corresponded to the weight of the tantalum oxide. It is assumed

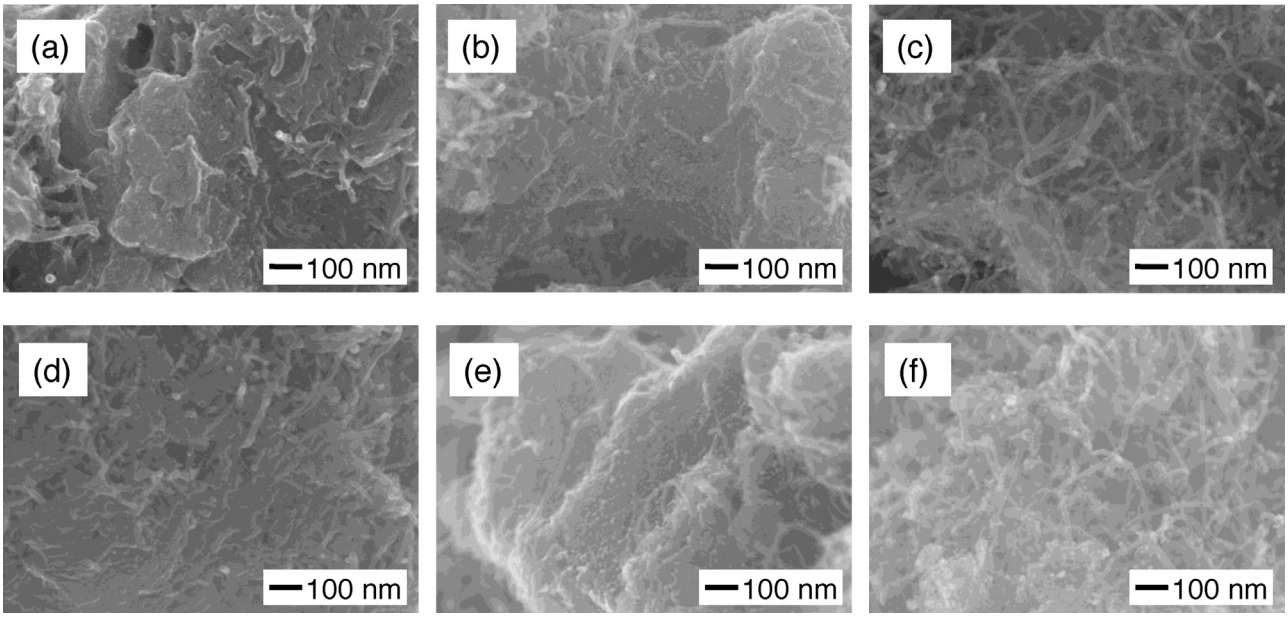

Fig. 11. SEM images of $TaC_xN_yO_z$/MWCNT_0.5%O_2 at (a) 0.5 h, (b) 1 h, and (c) 3 h; and $TaC_xN_yO_z$/MWCNT_0.05%O_2 at (d) 3 h, (e) 10 h, and (f) 15 h.

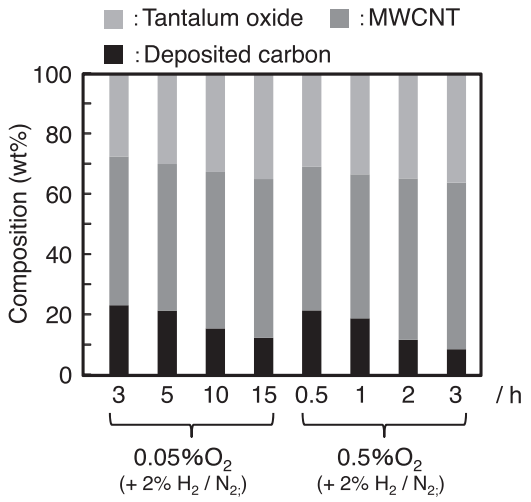

Fig. 12. Compositions of $TaC_xN_yO_z$/MWCNT_0.5%O_2 and $TaC_xN_yO_z$/MWCNT_0.05%O_2 after different oxidation times.

that the weight of the MWCNTs does not change during the oxidation under low oxygen partial pressure because the MWCNTs are considerably covered by the deposited carbon. Therefore, the weight of the MWCNTs was calculated from the quantity used during preparation. The weight of the deposited carbon was determined after deducting the oxide and MWCNT weights from the overall catalyst weight. Fig. 12 shows the compositions of the $TaC_xN_yO_z$/MWCNTs after different oxidation times. As predicted from the SEM images of Fig. 11, the amount of deposited carbon decreases with increasing oxidation time. The compositions of the $TaC_xN_yO_z$/MWCNTs with the same amounts of supplied oxygen (0.05% O_2 for 5 h and 0.5% O_2 for 0.5 h, and 0.05% O_2 for 10 h and 0.5% O_2 for 1 h) are nearly the same, suggesting that the extent of deposited carbon loss due to oxidation is determined not by the heat treatment time, but rather, the amount of the supplied oxygen. This is supported by the SEM images in Fig. 11(b) and (e): the morphologies of these $TaC_xN_yO_z$/MWCNTs, which had the same amount of supplied oxygen (0.05% O_2 for 10 h and 0.5% O_2 for 1 h), are similar.

The maximum ORR current density was obtained with the $TaC_xN_yO_z$/MWCNT_0.5%O_2-1 h catalyst (Fig. 11(b)). However, a large amount of aggregation due to carbon deposition was still observed. So, if the aggregation can be prevented, an enhancement in the ORR current density can be expected. The relationship between the amount of deposited carbon and $|j_{ORR}$@0.8 V| was obtained as shown in Fig. 13. The $|j_{ORR}$@0.8 V| reaches a maximum value at around 20 wt% deposited carbon. The deposited carbon influences the exposure of the surface of the oxides and the local electron conduction paths. For a small amount of deposited carbon, the local electron conductivity seems to be insufficient, although the exposure area of the oxide surface is increased. On the other hand, for a large amount of deposited carbon, the deposits cover the tantalum oxide and interfere with the ORR, although the local electron conductivity is probably high. Therefore, a moderate amount of deposited carbon is probably necessary to achieve a high ORR current density. Interestingly, both $TaC_xN_yO_z$/MWCNT_0.5%O_2 and 0.05%O_2 have maximum $|j_{ORR}$@0.8 V| values near 20 wt% deposited carbon. This result suggests that the exposure of the oxide surface and the formation of the electron conduction paths are similar for the same amount of supplied oxygen. The difference in the $|j_{ORR}$@0.8 V| values essentially reflects the state of the oxygen vacancies on the oxide surface.

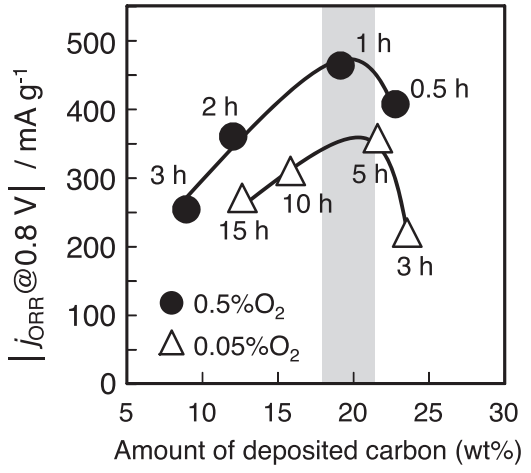

Fig. 13. Relationship between the amount of deposited carbon and j_{ORR} at 0.8 V.

4. Conclusions

To obtain high ORR activities in the tantalum oxide-based catalysts, we prepared catalysts from TaOPc, using MWCNTs as both a support and electroconductive material. We successfully obtained a dispersion of nano-sized tantalum oxide-based particles on the MWCNTs to increase the ORR current density. To clarify the factors which influence the ORR activity, we prepared the catalysts under different heat-treatment conditions and investigated the relationship between the physicochemical properties and the ORR activity, such as E_{ORR}@5 mA·g^{-1} and $|j_{ORR}$@0.8 V|. The values for E_{ORR}@5 mA·g^{-1} and $|j_{ORR}$@0.8 V| seemed to mainly reflect the quality and quantity of the active sites, respectively.

We found that the E_{ORR}@5 mA·g^{-1} increased with increasing crystalline distortion in the ortho. Ta_2O_5, experimentally observed as a shift and change in the FWHM of the Ta_2O_5 (0 0 1) peak. According to the RRDE measurements, the higher E_{ORR}@5 mA·g^{-1} indicated the preferential formation of active sites at which four-electron reduction occurs. Therefore, large crystalline distortions in the ortho. Ta_2O_5 produce high quality active sites (i.e. capable of four-electron reduction) for the ORR.

On the other hand, the $|j_{ORR}$@0.8 V| was affected by the surface area of the oxides and the formation of local electron conduction paths, which reflected the quantity of the active sites. The surface area and conduction paths were directly affected by the amount of deposited carbon. According to the calculated catalyst compositions, approximately 20 wt% carbon deposition was optimal for achieving high ORR current densities.

Acknowledgements

The authors thank Dainichiseika Color & Chemicals Mfg. Co., Ltd. for supplying the TaOPc, and the New Energy and Industrial Technology Development Organization (NEDO) for financial support.

Appendix A. Supplementary data

Supplementary data associated with this article can be found, in the online version, at http://dx.doi.org/10.1016/j.electacta.2015.03.125.

References

[1] F. Jaouen, V. Goellner, M. Lefevre, J. Herranz, E. Proietti, J.P. Dodelet, Oxygen reduction activities compared in rotating-disk electrode and proton exchange membrane fuel cells for highly active Fe N C catalysts, Electrochim. Acta 87 (2013) 619.

[2] Y. Nabae, Y. Kuang, M. Choka, T. Ichihara, A. Isoda, T. Hayakawa, T. Aoki, High performance Pt-free cathode catalysts for polymer electrolyte membrane fuel cells prepared from widely available chemicals, J. Mater. Chem. A 2 (2014) 11561.

[3] Y. Feng, A. Gago, L. Timperman, N. Alonso-Vante, Chalcogenide Metal Centers for Oxygen Reduction Reaction: Activity and Tolerance, Electrochim. Acta 56 (2011) 1009.

[4] J.Y. Cheon, T. Kim, Y.M. Choi, H.Y. Jeong, M.G. Kim, Y.J. Sa, J. Kim, Z. Lee, T.H. Yang, K. Kwon, O. Terasaki, G.G. Park, R. Radoslav, S.H. Joo, Ordered mesoporous porphyrinic carbons with very high electrocatalytic activity for the oxygen reduction reaction, Scientific reports 3 (2013) 2715.

[5] K. Lee, A. Ishihara, S. Mitsushima, N. Kamiya, K. Ota, Stability and Electrocatalytic Activity for Oxygen Reduction in WC+Ta catalyst, Electrochim. Acta 49 (2004) 3479.

[6] A. Ishihara, K. Lee, S. Doi, S. Mitsushima, N. Kamiya, M. Hara, K. Domen, K. Fukuda, K. Ota, Tantalum Oxynitride for a Novel Cathode of PEFC, Electrochem. Solid-State Lett. 8 (2005) A201.

[7] A. Ishihara, S. Doi, S. Mitsushima, K. Ota, Tantalum(Oxy)nitrides Prepared Using Reactive Sputtering for New Cathodes of Polymer Electrolyte Fuel Cell, Electrochim. Acta 53 (2008) 5442.

[8] K. Kikuchi, A. Ishihara, K. Matsuzawa, S. Mitsushima, K. Ota, Tantalum-based Compounds Prepared by Reactive Sputtering as a New Non-Platinum Cathode for PEFC, Chem. Lett. 38 (2009) 1184.

[9] Y. Liu, A. Ishihara, S. Mitsushima, N. Kamiya, K. Ota, Zirconium Oxide for PEFC Cathodes, Electrochem. Solid-State Lett. 8 (2005) A400.

[10] Y. Liu, A. Ishihara, S. Mitsushima, K. Ota, Influence of Sputtering Power on Oxygen Reduction Reaction Activity of Zirconium Oxides Prepared by Radio Frequency Reactive Sputtering, Electrochim. Acta 55 (2010) 1239.

[11] Y. Liu, A. Ishihara, S. Mitsushima, N. Kamiya, K. Ota, Transition Metal Oxides as DMFC Cathodes without Platinum, J. Electrochem. Soc. 154 (2007) B664.

[12] J.H. Kim, A. Ishihara, S. Mitsushima, N. Kamiya, K. Ota, Catalytic Activity of Titanium Oxide for Oxygen Reduction Reaction as a Non-Platinum Catalyst for PEFC, Electrochim. Acta 52 (2007) 2492.

[13] Y. Maekawa, A. Ishihara, S. Mitsushima, K. Ota, Catalytic Activity of Zirconium Oxynitride Prepared by Reactive Sputtering for ORR in Sulfuric Acid, Electrochem. Solid-State Lett. 11 (2008) B109.

[14] S. Doi, A. Ishihara, S. Mitsushima, N. Kamiya, K. Ota, Zirconium Based Compounds for New Cathode of Polymer Electrolyte Fuel Cell, J. Electrochem. Soc. 154 (2007) B362.

[15] J.H. Kim, A. Ishihara, S. Mitsushima, N. Kamiya, K. Ota, Oxygen Reduction Reaction of Ta–C–N Prepared by Reactive Sputtering with Heat Treatment, Electrochemistry 75 (2007) 166.

[16] A. Ishihara, M. Tamura, K. Matsuzawa, S. Mitsushima, K. Ota, Tantalum Oxide-Based Compounds as New Non-Noble Cathodes for Polymer Electrolyte Fuel Cell, J. Fuel Cell Sci. Technol. 8 (2011) 031005.

[17] Y. Ohgi, A. Ishihara, K. Matsuzawa, S. Mitsushima, M. Matsumoto, H. Imai, K. Ota, Oxygen Reduction Reaction on Tantalum Oxide-Based Catalysts Prepared from TaC and TaN, Electrochim. Acta 68 (2012) 192.

[18] Y. Ohgi, A. Ishihara, K. Matsuzawa, S. Mitsushima, M. Matsumoto, H. Imai, K. Ota, Factors for Improvements of Catalytic Activity for Zirconium Oxide-Based Oxygen–Reduction Electrocatalysts, J. Electrochem. Soc. 160 (2013) F162.

[19] A. Ishihara, M. Tamura, Y. Ohgi, M. Matsumoto, K. Matsuzawa, S. Mitsushima, H. Imai, K. Ota, Emergence of Oxygen Reduction Activity in Partially Oxidized. Tantalum Carbonitrides: Roles of Deposited Carbon for Oxygen-Reduction-Reaction-Site Creation and Surface Electron Conduction, J. Phys. Chem. C 117 (2013) 18837.